IMMUNOLOGY

A single-nucleotide polymorphism in a *Plasmodium berghei* ApiAP2 transcription factor alters the development of host immunity

Munir Akkaya[1]*, Abhisheka Bansal[2†], Patrick W. Sheehan[1‡], Mirna Pena[1], Alvaro Molina-Cruz[2], Lindsey M. Orchard[3], Clare K. Cimperman[1], Chen-Feng Qi[1], Philipp Ross[3§], Takele Yazew[1], Daniel Sturdevant[4], Sarah L. Anzick[4], Girija Thiruvengadam[2‖], Thomas Dan Otto[5], Oliver Billker[6,7], Manuel Llinás[3,8], Louis H. Miller[2], Susan K. Pierce[1]*

The acquisition of malaria immunity is both remarkably slow and unpredictable. At present, we know little about the malaria parasite genes that influence the host's ability to mount a protective immune response. Here, we show that a single-nucleotide polymorphism (SNP) resulting in a single amino acid change (S to F) in an ApiAP2 transcription factor in the rodent malaria parasite *Plasmodium berghei* (*Pb*) NK65 allowed infected mice to mount a T helper cell 1 (T_H1)–type immune response that controlled subsequent infections. As compared to *Pb*NK65^S, *Pb*NK65^F parasites differentially expressed 46 genes, most of which are predicted to play roles in immune evasion. *Pb*NK65^F infections resulted in an early interferon-γ response and a later expansion of germinal centers, resulting in high levels of infected red blood cell–specific T_H1-type immunoglobulin G2b (IgG2b) and IgG2c antibodies. Thus, the *Pb* ApiAP2 transcription factor functions as a critical parasite virulence factor in malaria infections.

INTRODUCTION

Malaria is an infectious disease caused by parasites of the genus *Plasmodium*. In humans, the most deadly parasite, *Plasmodium falciparum*, is responsible for the deaths of nearly 400,000 individuals a year, mostly young African children. A recent report by the World Health Organization concluded that the progress achieved over recent years in reducing global malaria cases and deaths appears to have stalled (*1*). At present, there is no effective malaria vaccine and the need for one is all the more acute. A better understanding of the host-parasite interactions that influence the host's ability to mount a protective immune response would aid in the development of an effective vaccine.

In previously unexposed individuals, blood-stage *P. falciparum* parasites rapidly replicate and induce fever and other symptoms of malaria, mediated by the parasite-induced production of pro-inflammatory cytokines, including interferon-γ (IFN-γ) and tumor necrosis factor–α (TNF-α), and chemokines by both innate immune cells and $CD4^+$ T cells (*2*–*5*). Although responsible for the disease symptoms, this inflammatory response is critical for the control of blood-stage parasites (*6*, *7*). Over time in malaria endemic areas, individuals eventually acquire protective antibodies that control blood-stage parasites. Thus, control of parasites in humans has two phases: an immediate inflammatory response upon infection and a longer-term process of acquiring protective antibodies following repeated infections. In nonlethal *Plasmodium* infections in mouse models, two similar phases, namely, an early IFN-γ–mediated control of blood-stage parasitemia followed by the later acquisition of protective antibodies, have been demonstrated (*8*–*10*). In lethal *Plasmodium* infections, these protective mechanisms are presumably not adequately induced, resulting in failure to control blood-stage parasitemia. At present, we have an incomplete understanding of the mechanisms that regulate the ability of *Plasmodium* parasites to induce the early inflammatory and later antibody responses in the host. Recent evidence suggests that *Plasmodium* parasites may disable the host's immune response through dysregulation of B cell and $CD4^+$ T cell functions (*11*, *12*), although specific mechanisms have yet to be demonstrated. This raises the question: does the *Plasmodium* parasite genome encode genes that function to control the host immune response, analogous to virulence factors in other pathogens. Currently, there are only a few examples of candidate virulence genes (*13*, *14*) and our understanding of the mechanisms by which such genes function is incomplete.

Here, we report on the impact of a single-nucleotide polymorphism (SNP) between the rodent parasites *P. berghei* (*Pb*) NK65 and *Pb*ANKA on the ability of mice to mount a protective immune response to infection. This SNP is in the gene that encodes a member of the apicomplexan homolog of plant Apetela2 (ApiAP2) transcription factor (TF) family. There are only 20 SNPs in the coding regions of the genes of *Pb*NK65 and *Pb*ANKA parasites (*14*). It is remarkable that the two parasites differ in so few SNPs considering the extreme differences in the diseases they cause. *Pb*NK65 infections result in anemia in mice that, with time, is lethal but not directly immune mediated. In contrast, *Pb*ANKA infections result in severe cerebral malaria that rapidly kills mice in a $CD8^+$ T cell–dependent process.

[1]Laboratory of Immunogenetics, National Institute of Allergy and Infectious Diseases, National Institutes of Health, Rockville, MD, USA. [2]Laboratory of Malaria and Vector Research, National Institute of Allergy and Infectious Diseases, National Institutes of Health, Rockville, MD, USA. [3]Department of Biochemistry and Molecular Biology and Huck Center for Malaria Research, The Pennsylvania State University, University Park, PA, USA. [4]Research Technologies Branch, National Institute of Allergy and Infectious Diseases, National Institutes of Health, Bethesda, MD, USA. [5]Wellcome Trust Sanger Institute, Hinxton, Cambridge CB10 1SA, UK. [6]Department of Molecular Biology, Umeå University, S-90187 Umeå, Sweden. [7]Laboratory for Molecular Infection Medicine Sweden, Umeå University, S-90187 Umeå, Sweden. [8]Department of Chemistry, Pennsylvania State University, University Park, PA, USA.
*Corresponding author. Email: spierce@nih.gov (S.K.P.); munir.akkaya@nih.gov (M.A.)
†Present address: School of Life Sciences, Jawaharlal Nehru University, New Delhi, India.
‡Present address: Department of Neurology, Washington University School of Medicine in St. Louis, St. Louis, MO, USA.
§Present address: Genetics, Genomics and Systems Biology Program, University of Chicago, Chicago, IL, USA.
‖Present address: Center for Genetic Medicine Research, Children's National Medical Center, Washington, DC, USA.

Thus, in the evolution of *Plasmodium*, these SNPs may have had a profound effect. Most of the 20 *Pb*NK65/*Pb*ANKA SNPs were in genes of unknown function. ApiAP2 was of interest because, as a TF, it likely controlled the expression of a variety of genes. We hypothesized that the *Pb*NK65/*Pb*ANKA SNP in the gene encoding ApiAP2 may be a good candidate for a parasite virulence factor that controls host immune responses.

There are 26 members of the ApiAP2 TF family, and despite their similarities, each has unique features in terms of their DNA recognition motifs and their expression patterns during the life cycle of *Plasmodium*, suggesting distinct functional properties (*15*–*17*). PBANKA_011210 (referred to here as ApiAP2) is a *Pb* ApiAP2 family member predominantly expressed in schizonts in the blood stage of the parasite infection in mice and appears to be essential as *Pb* parasites, in which the gene encoding ApiAP2 was knocked out, were not viable (*18*). Consequently, we have little knowledge of the functions that are dependent on the expression of this TF. Recent comparative genetic screening of rodent *Plasmodium* strains (*14*, *19*) revealed a nonsynonymous SNP (a T-to-C transition at position 5468) in the first DNA binding domain of the ApiAP2 gene. This SNP resulted in a phenylalanine (F) in *Pb*ANKA and *Pb*SP11 strains and a serine (S) in *Pb*NK65 and *Pb*K173 strains at amino acid position 1823 of the ApiAP2 protein. Given that this polymorphism is located in the ApiAP2 DNA binding domain and that the biochemical differences between phenylalanine, a hydrophobic aromatic amino acid, and serine, a hydrophilic amino acid, we postulated that these two genes may encode functionally different ApiAP2 proteins.

Here, we provide evidence that the two polymorphic forms of ApiAP2 do bind to different DNA motifs, resulting in altered transcriptional profiles, and that infections of mice by *Pb*NK65^{F} versus *Pb*NK65^{S} result in markedly different host immune responses, one that is protective and one that is not. Thus, this ApiAP2 is a *Pb* virulence factor.

RESULTS

The SNP in the DNA binding domain of *Pb* ApiAP2 alters its sequence specificity

We confirmed by DNA sequencing the presence of the SNP (T in *Pb*ANKA and C in *Pb*NK65-NYU at position 5468) in our laboratory clones of *Pb*ANKA and *Pb*NK65-NYU (fig. S1A). We cloned the sequences encoding the first AP2 DNA binding domain of each polymorphic form, expressed the genes in *Escherichia coli*, purified the proteins, and tested their DNA binding specificity using DNA binding microarrays composed of custom-made DNA sequences. The highest-scoring target DNA motifs for ApiAP2^{S} and ApiAP2^{F} were different: GGGCTTAA and GGGACTTA, respectively (Fig. 1A) (data file S1). To investigate the functional consequences of this ApiAP2 polymorphism, we generated *Pb*NK65 parasites that differed only in the T5468C SNP using CRISPR-Cas9 (fig. S1, B and C). The whole-genome sequence analysis of wild-type (WT) *Pb*NK65 and CRISPR-edited *Pb*NK65 parasites confirmed that the only 10 SNP regions that were consistently different between the two parasites were the target-specific alterations generated by the CRISPR strategy. This included nine silent mutations generated by the guide sequence and one missense mutation, resulting in the desired S-to-F alteration (table S1). SNPs that were observed only in a fraction of reads of the same gene were excluded, as alternate sequences were similarly present in both parasites.

We refer to the *Pb*NK65 strain that carries C at nucleotide position 5468 resulting in an S at amino acid position 1823 in the ApiAP2 protein as *Pb*NK65^{S} and, conversely, the *Pb*NK65 strain that has a T at position 5468 resulting in an F at position 1823 in the ApiAP2 protein as *Pb*NK65^{F}. We infected mice with either *Pb*NK65^{F} or *Pb*NK65^{S} and carried out an RNA-sequencing (RNA-seq) analysis on blood drawn from each when parasitemias reached approximately 10% and the distributions of various blood-stage forms were comparable. A principal components analysis of the data showed that the transcriptomes of the *Pb*NK65^{S} and *Pb*NK65^{F} parasites overlapped (Fig. 1B). However, a detailed RNA-seq analysis showed differential expression of 46 *Plasmodium* genes, 40 of which were down-regulated in *Pb*NK65^{F} compared to *Pb*NK65^{S} (Fig. 1C). Among these differentially expressed 46 genes, 22 belonged to the interspersed repeat (IR) of the *Berghei* IR (BIR) gene family (Fig. 1D). The *Plasmodium* IR family (PIR), the largest gene family in *Plasmodium*, consists of subtelomeric genes that are thought to encode proteins expressed on the infected red blood cell (iRBC) surface and play a major role in antigenic variation in the parasite (*20*). The RNA-seq data also showed differences in the expression levels of *Plasmodium* genes belonging to three additional gene families, fam-a (7 of 46), fam-b (8 of 46), and fam-c (2 of 46) (Fig. 1D). These genes, like the BIRs, are expressed predominantly in blood stage and are thought to be exported to the iRBC surface and possibly play roles in invasion, antigenic variation, and immune evasion (*14*, *21*, *22*).

We carried out a genome-wide analysis to determine whether the DNA binding motifs of ApiAP2^{S} and ApiAP2^{F} were present in the promoter regions of the differentially expressed genes identified by RNA-seq. Because of high redundancy in the first and the eighth nucleotides of the identified DNA binding motifs (Fig. 1A), we focused on the middle six nucleotides and tested the presence of these two motifs within the promoter regions arbitrarily defined as the 1500 base pairs (bp) before the start site of each gene, in all genes in the *Pb* genome. This algorithm identified 113 possible binding sites for ApiAP2^{S} and 75 for ApiAP2^{F} in the promoters of the 46 differentially regulated genes (data file S1). Thus, the ApiAP2^{S} motif was in higher frequency as compared to the ApiAP2^{F} motif. Among these 46 genes, 42 contained at least one ApiAP2^{S} or ApiAP2^{F} DNA binding motifs, providing a link between the SNP and the differential regulation of these genes. An in-depth analysis of the promoter regions that contained these motifs showed that although the distribution of the two motifs within the promoters of all *Pb* genes was comparable (Fig. 1E), within the differentially expressed genes, the ApiAP2^{S} motifs tended to be located more proximal to the transcription start site as compared to the ApiAP2^{F} motifs (Fig. 1F), suggesting possible differences in transcriptional regulation of these genes by ApiAP2^{S} and ApiAP2^{F}. Together, these analyses provide a link between the presence of the ApiAP2^{S} and ApiAP2^{F} DNA binding motifs in the promoter regions and the differential expression of these genes in *Pb*NK65^{S} and *Pb*NK65^{F} parasites.

PbNK65^{F} parasites are able to complete both the sexual stages in the mosquito host and the pre-erythrocytic stage in the mouse

We determined whether the *Pb*NK65^{F} parasite was able to complete the full life cycle of the parasite. The cycle begins with the differentiation of sexual-stage gametocytes in the mouse host that are taken up in a blood meal by mosquitoes. In the mosquito midgut, the gametes form oocysts that then develop into sporozoites, a highly motile form

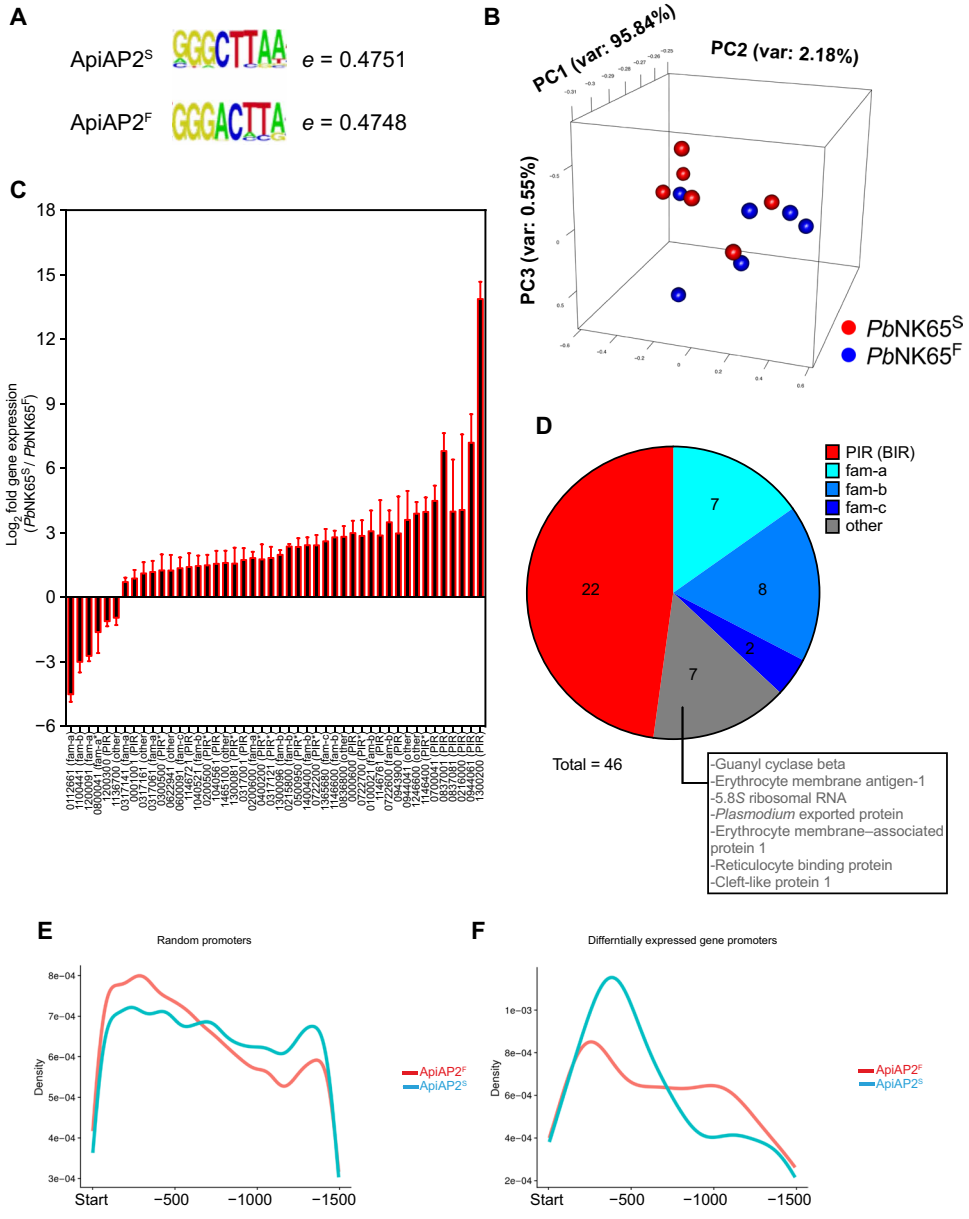

Fig. 1. ApiAP2^F mutation alters the DNA sequence specificity of the PBANKA_011210 ApiAP2 protein. (**A**) DNA sequences that received the highest hit in DNA binding microarray analysis of the first domain of ApiAP2^S- and ApiAP2^F-mutated PBANKA_011210 ApiAP2 proteins. (**B** to **D**) *Pb*NK65^S or *Pb*NK65^F parasites were used to infect C57BL/6 mice. RNA-seq analysis was carried out from blood samples of infected mice. Principal components analysis (B), genes whose expressions were significantly altered between the two groups (C), and the pie chart representation of multigene families that these genes belong to (D) are shown. Numbers under bar graphs in (C) indicate the gene annotation in (PBANKA_######) format. Gene families for each gene are indicated in parenthesis. Pseudogenes are shown with asterisks. (**E** and **F**) Density graphs showing the relative distribution of the middle hexamer regions of DNA sequences in (A) in the 1500-bp promoter region of randomly sampled (E) or differentially regulated (F) genes.

of the parasite that accumulates in the mosquito salivary glands. The sporozoites are injected into the mouse host as the mosquito takes a blood meal and travel through the blood to the liver where they infect hepatocytes. In the liver, the sporozoites expand and differentiate to merozoites that exit the liver and begin the blood-stage infection, thus completing the life cycle. To determine whether the SNP in ApiAP2 affected the ability of the parasite to complete its life cycle, we devised an experimental model that included the sexual and pre-erythrocytic stages of the *Pb* infection (fig. S2A). Mice were infected with *Pb*NK65^S or *Pb*NK65^F (10^6 iRBCs intraperitoneally), and once the parasitemia reached approximately 1.2%, mosquitoes were fed on these mice. At 14 days after feeding, a subset of mosquitoes was dissected and the oocysts in midgut were evaluated both qualitatively (fig. S2B) and quantitatively (fig. S2C). A portion of the remaining mosquitoes were dissected at day 21 after feeding; sporozoites in their salivary glands were harvested and counted (fig. S2D). Sporozoites (5×10^3) were injected into uninfected mice, and the progression to liver-stage malaria was observed by harvesting

liver at 46 hours after injection and comparing the parasite levels by quantitative polymerase chain reaction (qPCR) (fig. S2E). None of these parameters showed variation between *Pb*NK65^S and *Pb*NK65^F. Last, the *Plasmodium*-infected mosquitoes were fed on uninfected mice, and the progression of disease was observed. While notable experimental variation existed in disease progression either due to the inability to control the inoculum size or due to an unidentified difference in sporozoite function, all infected mice eventually developed blood-stage infection, as confirmed by repeated parasitemia checks (data not shown). These findings indicate that the SNP in the ApiAP2 does not prevent the completion of the full plasmodium life cycle.

Infection with *Pb*NK65^F drives a strong T_H1-type immune response

To explore the impact of the SNP in ApiAP2 on the outcome of blood-stage infection, we infected mice with either *Pb*NK65^S- or *Pb*NK65^F-infected RBCs at 10^6 parasites per mouse. The hemoglobin levels, parasitemias, and survival for mice infected with the two different parasites were similar (Fig. 2, A to C). All mice died because

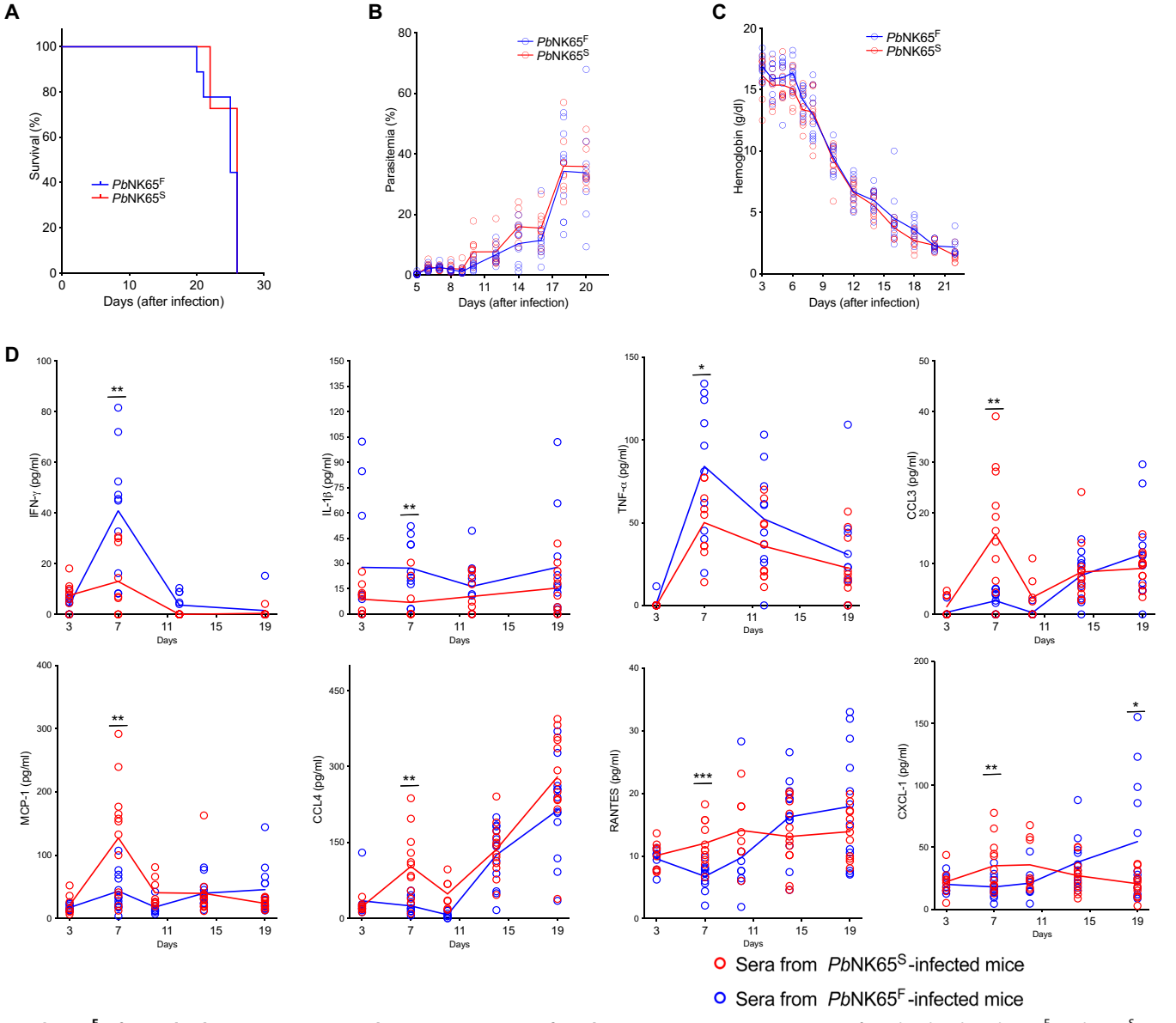

Fig. 2. *Pb*NK65^F infection leads to stronger IFN-γ and TNF-α responses in infected mice. (**A** to **C**) C57BL/6 mice were infected with either *Pb*NK65^F or *Pb*NK65^S using 10^6 iRBCs per mouse delivered intraperitoneally. Changes in survival (A), parasitemia (B), and hemoglobin levels (C) were monitored during the course of infection. Each circle represents an individual mouse. Data represent three independent experiments each carried out with at least 10 animals per group. (**D**) Sera collected at different time points of mice infected, as described above. Time-dependent changes in serum levels of various cytokines and chemokines are quantified using a multiplex enzyme-linked immunosorbent assay (ELISA) strategy. Data represent two independent experiments. Each circle refers to a single mouse and lines denote mean values. Statistically significant differences are shown with asterisk (* = $0.01 < P \leq 0.05$; ** = $0.001 < P \leq 0.01$; *** = $0.0001 < P \leq 0.001$). Statistical significance was calculated using Welch's *t* test (F)

of severe anemia between days 20 and 26 after infection, with parasitemias between 30 and 60% and hemoglobin levels below 3 g/dl. To characterize the early immune response in *Pb*NK65^S- and *Pb*NK65^F-infected mice, we collected sera on days 3, 7, 11, 15, and 19 after infection and assayed these for various cytokines and chemokines (Fig. 2D). The serum levels of IFN-γ, the master enhancer of T helper cell 1 (T_H1) differentiation, were higher in *Pb*NK65^F-infected mice as compared to *Pb*NK65^S-infected mice, peaking on day 7 after infection. Similarly, on day 7 after infection, the levels of interleukin-1β (IL-1β) and TNF-α, cytokines that also enhance T_H1 cell differentiation, were higher in *Pb*NK65^F-infected mice. Conversely, on day 7 after infection, the levels of the proinflammatory regulators and chemoattractants such as CXCL-1, CCL3, CCL4, MCP-1, and RANTES were higher in *Pb*NK65^S-infected mice as compared to *Pb*NK65^F-infected mice. With time after infection, the levels of CCL4 became equivalent in the two groups of mice and continued to increase through day 19 after infection. For CCL3, MCP-1, RANTES, and CXCL-1, as the infection progressed to day 19 after infection, the level of these cytokines tended to reverse and increased more in *Pb*NK65^F-infected mice as compared to *Pb*NK65^S-infected mice. Levels of IL-10 and IL-12 p40 were also increased with infection but were not significantly different between the two groups of mice (fig. S3).

Infection with *Pb*NK65^F results in a persistent adaptive immune response

To characterize the immune response to infection by *Pb*NK65^F and *Pb*NK65^S, we collected spleens of the mice at day 6, 10, 15, or 19 after infection and quantified the total numbers of germinal center (GC) B cells (Fig. 3A), B cells of the plasma cell (PC) lineage (Fig. 3B), and follicular helper T (T_{FH}) cells (Fig. 3C) using the gating strategy outlined in fig. S3A. The numbers of GC B cells, PC lineage cells, and T_{FH} cells peaked similarly around day 10 to 15 after infection in both *Pb*NK65^S- and *Pb*NK65^F-infected mice. However, in the late stage of the infection on day 19 after infection, although all three cell populations decreased in numbers in both *Pb*NK65^S- and *Pb*NK65^F-infected mice, the numbers of GC B cells, PC lineage cells, and T_{FH} cells were significantly higher in *Pb*NK65^F-infected mice as compared to *Pb*NK65^S-infected mice, indicating a more persistent immune response (Fig. 3, A to C). We also assessed the total number of $CD8^+$ T cells, as well as the numbers of $CD8^+$ effector memory and central memory T cells 10 and 19 days after infection and observed no differences in these numbers in *Pb*NK65^S-infected versus *Pb*NK65^F-infected mice (fig. S3B).

To determine whether the persistent increases in GC B cells, PC, and T_{FH} in response to *Pb*NK65^F infections were dependent on IFN-γ, we compared responses to infection by either *Pb*NK65^S or *Pb*NK65^F in IFN-γ–deficient mice (IFN^{KO} mice) and WT mice at day 19 after infection. Although infections with *Pb*NK65^S and *Pb*NK65^F (10^6 parasites per mouse) were fatal in both mouse strains, we observed differences in the expansion of GC B cells, PC lineage cells, and T_{FH} cells in IFN^{KO} mice as compared to WT mice 19 days after infection. In IFN^{KO} mice, *Pb*NK65^F infection resulted in fewer GC B cells, PC lineage B cells, and T_{FH} cells as compared to *Pb*NK65^S infection (Fig. 3, D to F), a reversal of the phenomenon observed in infection of WT mice (Fig. 3, A to C). Thus, the ability of *Pb*NK65^F infections to expand lymphocyte populations was IFN-γ dependent. In addition, we observed differences in the magnitude of the expansion of cells in WT versus IFN-γ knockout (KO) mice (Fig. 3, D to F) that may be explained by the immunomodulatory role of B cell–intrinsic IFN-γ signaling as recently shown by Guthmiller *et al.* (*23*).

The splenic architecture has been shown to be disrupted in the acute blood stage of malaria, primarily due to a combination of the burden of iRBC in the spleen and erythropoiesis (*24*–*26*). We carried out a histopathological evaluation of spleens taken from *Pb*NK65^S- and *Pb*NK65^F-infected mice. On day 10 after infection, the spleens of *Pb*NK65^S- and *Pb*NK65^F-infected mice were similar with well-organized B cell follicles, as visualized by double staining with CD4- and B220-specific antibodies (Fig. 4, A and C). Numerous peanut agglutinin (PNA)–stained GC foci with proliferative activity (Ki-67^+) were also present in mice infected with *Pb*NK65^S and *Pb*NK65^F. However, at the late stage of infection, 19 days after infection, significant disruption of the B cell follicle structure was observed in *Pb*NK65^S-infected mice with no visible B-T organization, no typical GCs, and no proliferative activity (Fig. 4, B and C). In contrast, in *Pb*NK65^F-infected mice, B-T organization, GCs, and proliferative activity persisted, consistent with the flow cytometry data indicating a prolonged cellular response (Fig. 4, B and C).

Having observed a more persistent GC B cell and PC response in *Pb*NK65^S-infected versus *Pb*NK65^F-infected mice, we measured the levels of total and iRBC-specific immunoglobulin M (IgM) and IgG at days 7 and 19 after infection (Fig. 5A). The sera obtained on days 7 and 19 after infection showed similar levels of total IgM in *Pb*NK65^S- and *Pb*NK65^F-infected mice (Fig. 5A). However, on day 19 after infection, the levels of total IgG were significantly higher in the *Pb*NK65^F-infected mice compared to *Pb*NK65^S-infected mice (Fig. 5A). We also measured the levels of IgM and IgG that bound to lysates of uninfected RBCs or to lysates prepared from either *Pb*NK65^F- or *Pb*NK65^S-infected RBCs. Antibody reactivity against uninfected RBC lysate was observed, indicating a degree of autoreactivity consistent with earlier reports (fig. S4A) (*27*, *28*). However, the levels of uninfected RBC binding antibodies were around $^1/_5$ to $^1/_{10}$ of the level of iRBC binding antibodies. We subtracted the values obtained from uninfected RBC lysate–coated wells from the values acquired from the corresponding iRBC lysate–coated wells and presented these values (Fig. 5, B to G). The levels of iRBC-specific IgM were similar between mice infected with *Pb*NK65^S or *Pb*NK65^F on both days 7 and 19 after infection (Fig. 5B). In contrast, the iRBC-specific IgG was significantly higher on day 19 after infection (but not on day 7 after infection) in *Pb*NK65^F-infected mice as compared to *Pb*NK65^S-infected mice regardless of the source of the iRBC lysate (Fig. 5C). The higher total levels of iRBC-specific IgG reflected increases in the levels of IgG2b (Fig. 5E) and IgG2c (Fig. 5F) but not of IgG1 (Fig. 5D) or IgG3 (Fig. 5G), indicating a predominant T_H1-type immune response to the *Pb*NK65^F parasites, consistent with the observation of an early T_H1-type inflammatory response. Differences in anti-iRBC antibody levels between *Pb*NK65^F- and *Pb*NK65^S-infected mice may reflect increases in antibodies against the same parasite target molecules and/or differential expression of immunogenic molecules between the parasite strains, leading to different antibody repertoires.

Reduction in parasite burdens in *Pb*NK65^F infections, but not in *Pb*NK65^S infections, allows development of protective immunity

Having observed that lethal infection of mice with *Pb*NK65^F resulted in immune responses late in the infection just before death of the mice, we determined whether reducing the parasite burden during

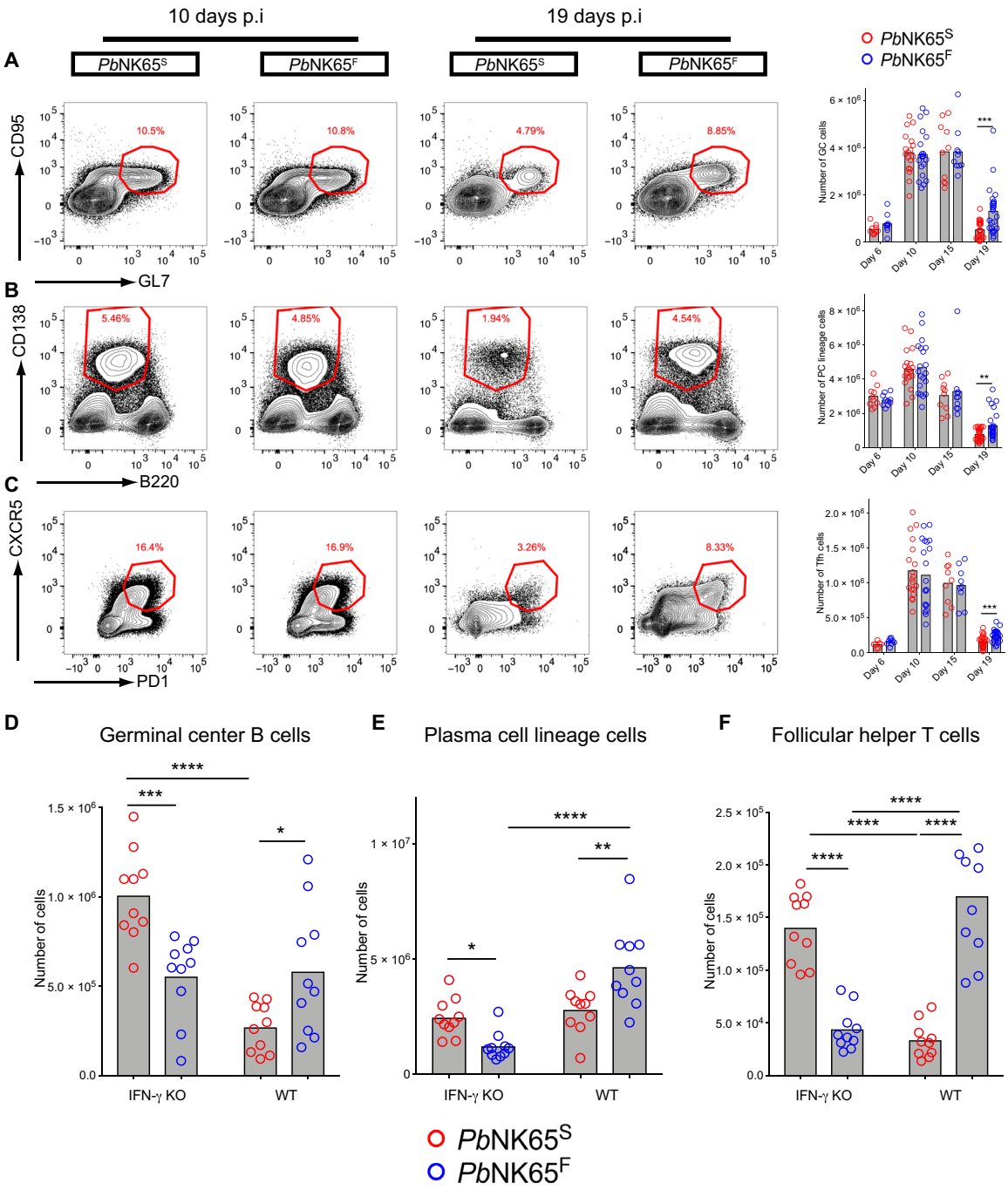

Fig. 3. *Pb*NK65^F-induced IFN-γ is linked to formation of stronger adaptive immune responses. (**A** to **C**) C57BL/6 mice were infected with either *Pb*NK65^F or *Pb*NK65^S using 10^6 iRBCs per mouse delivered intraperitoneally. Spleens were harvested at different time points, and GC B cells within the B cell gate (A), plasma cell (PC) lineage cells within the splenocyte gate (B), and T_{FH} within the T_H gate (C) are analyzed in flow cytometry. Representative flow cytometry plots (left) and bar graphs of actual cell numbers (right) are shown for each cell type. Data are pooled from four independent experiments. p.i., post-infection. (**D** to **F**) Age- and sex-matched IFN-γ KO and WT (C57BL/6) mice were infected side by side with either *Pb*NK65^F or *Pb*NK65^S as outlined above. Mice were sacrificed at day 19 after infection, and their spleens were analyzed. Each circle represents an individual mouse. Bars indicate the mean values. Statistical significance was calculated using Welch's *t* test (A to C) or one-way analysis of variance (ANOVA) with Sidak's multiple comparison test (D to F). Significant values are shown with asterisks (* = 0.01 < $P \leq 0.05$; ** = 0.001 < $P \leq 0.01$; *** = 0.0001 < $P \leq 0.001$).

the initial infection would allow protective immunity to fully develop in *Pb*NK65^F-infected mice and promote survival. We reduced the parasite burden by either treating infected mice with a nonsterilizing dose of chloroquine (Fig. 6, A to D) or by reducing the parasite inoculum (Fig. 6, E to G).

For chloroquine-mediated reduction in parasite load, as depicted (Fig. 6A), mice were infected with either *Pb*NK65^S or *Pb*NK65^F, the infections were allowed to progress for 8 days, and parasitemias were quantified by flow cytometry and confirmed blood smears. At day 8 after infection, mice were randomly divided into two groups

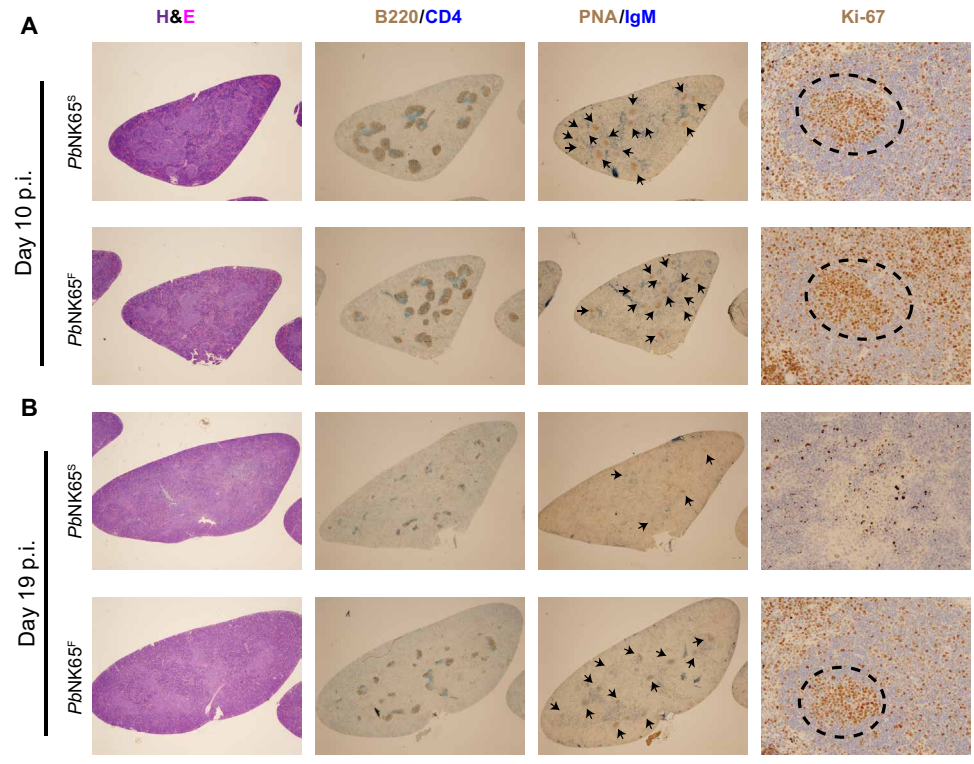

C

		GC reaction	GC proliferation	T_{FH}
Day 6 p.i.	*Pb*NK65^S	++	++	++
	*Pb*NK65^F	++	++	++
Day 10 p.i.	*Pb*NK65^S	++	++	++
	*Pb*NK65^F	++	++	++
Day 15 p.i.	*Pb*NK65^S	++	++	++
	*Pb*NK65^F	+++	+++	++
Day19 p.i.	*Pb*NK65^S	No typical GC	No proliferation	–
	*Pb*NK65^F	+	+	+

Legend
(–) None, (+) Minimal, (++) Moderate, (+++) Abundant

Fig. 4. Infection with *Pb*NK65^F causes more persistent GC response and less disruption in splenic architecture. Mice were infected as outlined in Fig. 2. Spleens harvested at different time points were stained with hematoxylin and eosin (H&E) to show overall splenic structure, B220/CD4 to localize follicles, PNA/IgM to point out the GC foci, and Ki-67 to determine the proliferation activity in GCs. Representative spleen sections belonging to either *Pb*NK65^S parasite– or *Pb*NK65^F parasite–infected mice are shown for day 10 (**A**) and day 19 (**B**). Arrowheads and dashed circles indicate GC foci and proliferative activity, respectively. (**C**) Histopathologic evaluation of the spleen samples taken on days 6, 10, 15, and 19 after infection of mice with either *Pb*NK65^S or *Pb*NK65^F and processed as described above. At least two mice were evaluated per group per day. p.i., postinfection.

that were either left untreated or treated daily for 8 days with the anti-malarial chloroquine at nonsterilizing doses. Survival and parasite levels were followed until day 75 after infection. In the absence of chloroquine, the parasite levels increased in both *Pb*NK65^S- and *Pb*NK65^F-infected mice, reaching high levels (Fig. 6B), resulting in the death of all the mice by day 23 (Fig. 6C). The 8-day chloroquine treatment reduced the parasitemia to nearly undetectable levels in both *Pb*NK65^S- and *Pb*NK65^F-infected mice (Fig. 6B). Once the daily chloroquine treatment was stopped, on day 16 after infection, recrudescent parasitemias were not controlled in most *Pb*NK65^S-infected mice and reached high levels (Fig. 6B), resulting in the death of 80% of the mice by day 40 after infection (Fig. 6C). In contrast, most *Pb*NK65^F mice controlled the recrudescent parasitemia, maintaining it at low levels (Fig. 6B), resulting in survival of over 90% of these mice (Fig. 6C).

To determine whether *Pb*NK65^F-infected, chloroquine-treated mice that survived developed protective immunity, in a parallel experiment, we challenged a group of the surviving mice, which were free of parasite as confirmed by blood smear at day 37 after infection, with either *Pb*NK65^F or *Pb*NK65^S parasites (Fig. 6D). Age-matched mice that did not receive the first infection but were treated or not with chloroquine served as controls (Fig. 6D and fig. S4B). All infected control mice died by day 27 after infection (Fig. 6D). In contrast, 100% of mice that survived the first infection by *Pb*NK65^F following chloroquine treatment survived the challenge infection with *Pb*NK65^F and 60% were protected against challenge with *Pb*NK65^S. Repeated experiments confirmed these findings despite slight alterations in the duration of chloroquine treatment required to sufficiently limit parasitemia. Thus, *Pb*NK65^F infections in which the parasite burden was reduced resulted in complete protection against

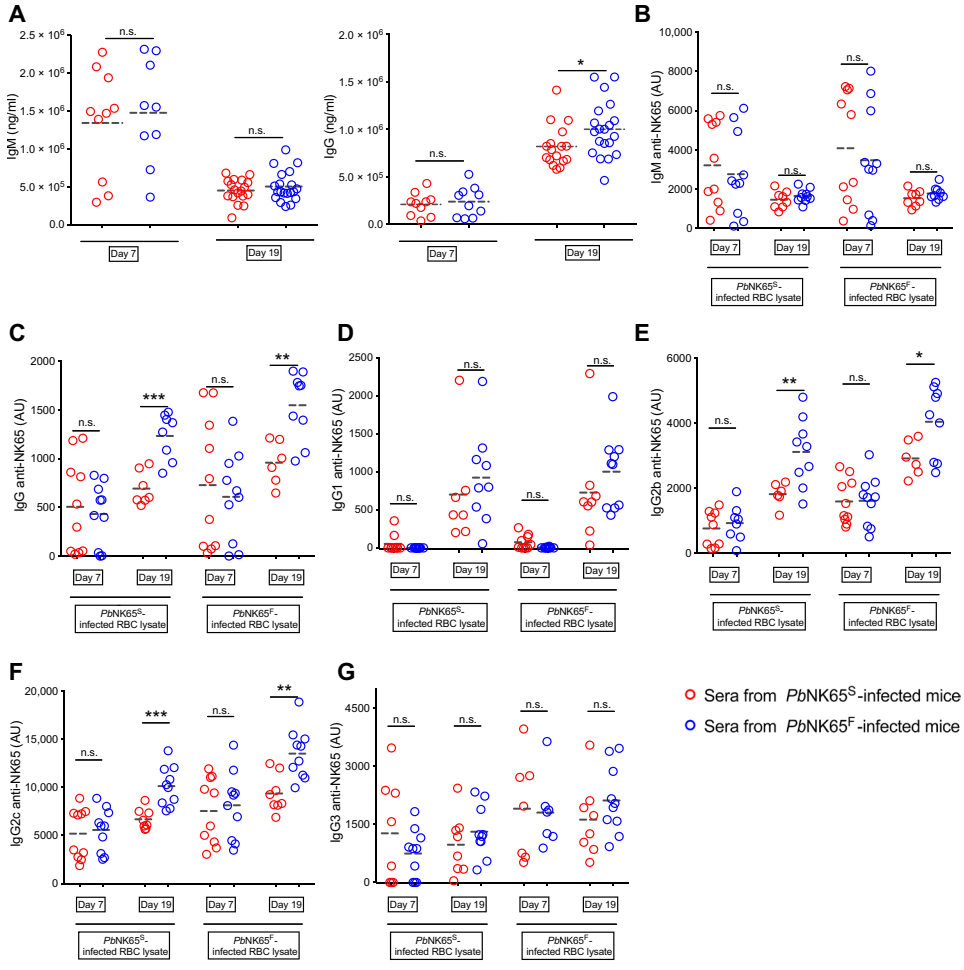

Fig. 5. *Pb*NK65^{F} infection leads to a stronger T_H1 type immune response. (**A** to **G**) C57BL/6 mice were infected with either *Pb*NK65^{F} or *Pb*NK65^{S} as described in Fig. 2. Sera were collected at days 7 and 19 after infection and were assayed for total IgM and IgG (A) using ELISA kits. Parasite-specific IgM (B), IgG (C), IgG1 (D), IgG2b (E), IgG2c (F), and IgG3 `(G) were quantified on ELISA plates coated with iRBC lysates of WT parasite– or mutant parasite–infected mice. Arbitrary units (AU) were calculated using a titration curve generated by serially diluting a mixture of serum samples as explained in Materials and Methods. n.s. = $P > 0.05$; * = $0.01 < P \leq 0.05$; ** = $0.001 < P \leq 0.01$; *** = $0.0001 < P \leq 0.001$ (Welch's *t* test).

challenge with *Pb*NK65^{F} and partial protection to the highly related *Pb*NK65^{S} strain.

We reduced the parasite burden by reducing the parasite inoculum (Fig. 6, E to G). We first titrated the dose of iRBC from 10^6 to 10^1 in 10-fold increments to determine whether there was a dose of iRBCs at which *Pb*NK65^{F}-infected mice survived and *Pb*NK65^{S}-infected mice did not. We found that this occurred at a dose of 10^2 iRBCs per mouse and that, above this dose, both infections were lethal and, below this dose, mice survived both infections. At a dose of 10^2 iRBC per mouse, 70% of the *Pb*NK65^{F}-infected mice did not develop detectable levels of parasitemia (Fig. 6E), and these mice survived the infection (Fig. 6F). In contrast, all of the *Pb*NK65^{S}-infected mice developed parasitemias (Fig. 6E), and none of these mice survived. Thus, mice were able to mount a protective response against the *Pb*NK65^{F} parasites but not against *Pb*NK65^{S}. Moreover, survival of the *Pb*NK65^{F} infection was dependent on IFN-γ, as in IFN^{KO} mice, parasitemias were not controlled in *Pb*NK65^{S} and *Pb*NK65^{F} infections and all mice died (fig. S4C). This finding is consistent with the observation that *Pb*NK65F infections resulted in higher IFN-γ responses as compared to *Pb*NK65S infections at day 7 after infection.

To ensure that the differential progression of disease between *Pb*NK65^{F}- and *Pb*NK65^{S}-infected mice was dependent on the adaptive immune response and not due to intrinsic growth properties of the parasites, we infected WT mice and mice deficient in RAG-2 (RAG-2^{KO}) that lacked an adaptive immune system. In RAG-2^{KO} mice, the parasitemias in *Pb*NK65^{S} and *Pb*NK65^{F} infection progressed similarly to high levels (Fig. 6G). Thus, the ability to control parasitemia in the low-inoculum *Pb*NK65^{F} infection was lost in RAG-2^{KO} mice.

DISCUSSION

Malaria continues to be a serious global health problem, affecting over 200 million people each year and causing over 400,000 deaths annually in Africa alone (*29*). At present, we do not have an effective malaria vaccine and a clear understanding of the genetic factors that govern *Plasmodium* virulence would likely contribute to development

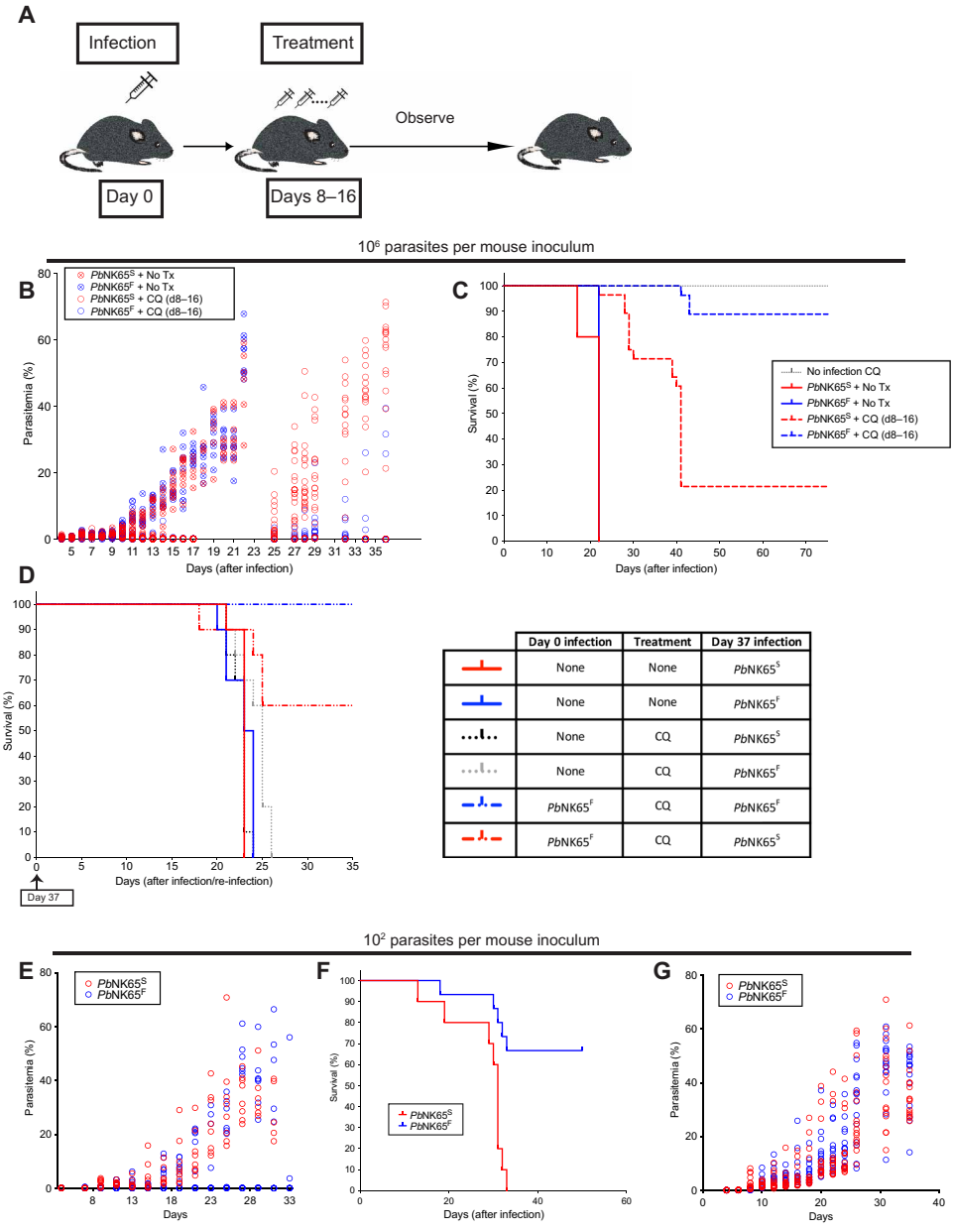

Fig. 6. The SNP affects the disease progression and formation of immunologic memory in infected mice. (**A** to **D**) C57BL/6 mice were infected with 10^6 iRBCs (intraperitoneally) coming from either *Pb*NK65^F- or *Pb*NK65^S-infected donors. A group of mice were treated with chloroquine (10 mg/kg) daily between days 8 and 16 after infection, after which the treatment was ceased and disease progression was observed. The experimental design is illustrated in (A). Progression of parasitemia (B) and Kaplan-Meier survival curve (C) for the initial infection are shown. (D) In a parallel experiment, some of the surviving mice (after being confirmed as parasite free by blood smear) were re-infected on day 37 and observed until day 80. Kaplan-Meier survival chart (left) of the groups of mice that were infected 10^6 iRBCs (intraperitoneally) as outlined in the table (right) is shown. (**E** to **G**) C57BL/6 (E and F) or RAG-2 KO (G) mice were infected with 10^2 iRBCs (intraperitoneally) taken from either *Pb*NK65^S- or *Pb*NK65^F-infected donors. The parasitemia (E) and survival (F) curves of infected C57BL/6 mice and parasitemia curves of infected RAG-2 KO mice are shown. Data represent two independent experiments each carried out with 10 to 15 mice per group. Circles refer to individual mice.

of a vaccine. Here, we provided evidence that a single SNP in the AP2 DNA binding domain of the TF ApiAP2 is a virulence factor in the mouse malaria parasite *Pb*NK65. Mice are not able to mount a protective immune response to *Pb*NK65^S parasites and develop high parasitemias and die even at low-inoculum infections (100 parasites per infection). In contrast, *Pb*NK65^F infections induce an early IFN-γ response and a later expansion of GC B cells, PCs, and T_{FH} cells, resulting in high levels of iRBC-specific T_H1-type $IgG2_b$ and $IgG2_c$ antibodies. The expansion of B cells, PCs, and T_{FH} and the ability to survive low-inoculum infections are IFN-γ dependent, as shown in IFN-γ^{KO} mice.

In terms of possible mechanisms by which expression of ApiAP2^F confers the ability of *Pb*NK65^F to induce a protective immune response, we showed that the nonsynonymous SNP altered the target DNA sequence of ApiAP2^F, resulting in the differential expression of 46 *Pb* genes in the blood-stage infection. Although the individual

functions and expression patterns of these genes are largely unknown, comparative genomic analyses predict expression on the RBC surface and thus involvement in host-pathogen interactions (*14*, *20*). Twenty-two of the 46 differentially expressed genes are members of the BIR/PIR family that are thought to play an important role in antigenic variation on the iRBC surface. The expression of ApiAP2^{F} resulted in the down-regulation of the transcription of the majority of these genes in *Pb*NK65^{F} infection. Thus, our data suggest that these BIR genes may play a role in either suppressing or evading the immune response in *Pb*NK65^{S} infections. Spence *et al.* (*30*) recently provided evidence that vector transmission intrinsically modified the asexual blood-stage infection of *P. chabaudi chabaudi*, resulting in an enhanced, protective immune response in mice. The attenuated virulence of vector-transmitted *P. chabaudi chabaudi* was associated with increased expression of members of the CIR/PIR family. Thus, in this case, the PIR genes appear to be a target of the immune response. The role of these gene families in parasite virulence will require a better understanding of their function and expression.

Our results suggest that ApiAP2^{S} expression is beneficial to the parasite in preventing protective immune responses in the infected host. The ApiAP2^{S} SNP is highly conserved in ApiAP2 orthologs in almost all *Plasmodium* strains, including the human parasite *P. falciparum*. Moreover, the target DNA sequence we report here for domain 1 of ApiAP2^{S} is also conserved in the AP2 domain of the *P. falciparum* ortholog, namely, PF3D7_0613800 (*15*), suggesting that the conservation of this SNP is due to the immune invasion benefit it confers on the parasite.

Conversely, ApiAP2^{F} expression is presumably deleterious to the parasite, as its expression evokes a parasite-specific immune response in the host. Nevertheless, ApiAP2^{F} is encoded in at least two strains of *Pb* (*19*). It is of interest that whole-genome sequencing of multiple laboratory *Plasmodium* strains showed that parasite strains that differed in approximately 20 SNPs in their entire coding regions, including in the ApiAP2 SNP described here, had dramatically different outcomes in infection, resulting in severe anemia versus cerebral malaria (*14*). Understanding the relationship of the immune response to parasites expressing ApiAP2^{F} in different parasite backgrounds and disease pathology will be of interest.

In conclusion, through in-depth functional characterization, we identify the ApiAP2 PBANKA_011210 as an important regulator of the *Pb* immune evasion machinery. To our knowledge, this is not only the first report of a role for any ApiAP2 family member in a mammalian host-pathogen interaction but also the first characterization of a functional role for an essential ApiAP2. The approach described here may facilitate functional characterization of other essential members of the ApiAP2 family for which KO parasites are not viable.

MATERIALS AND METHODS

Mice and reagents

For all animal experiments, age-matched, 7- to 9-week-old female mice were used. C57BL/6 mice were purchased from The Jackson Laboratory. RAG-2 KO and IFN-γ KO mice were purchased Taconic Farms. Mice were maintained at the National Institute of Allergy and Infectious Diseases animal facility according to Animal Care and Use Committee Standards.

Fluorescent-conjugated monoclonal antibodies against mouse CD45 [allophycocyanin (APC)], Ter119 (APC-Cy7), CD19 [phycoerythrin (PE)–Cy7], B220 (AF700), CD138 (PE), CD4 (BV605), CXCR5 (BV421), PD-1 (PE), CD8 (BV785), CD44 (AF700), and CD62L (PE-Dazzle 594) were purchased from BioLegend. Anti-mouse GL7 (e660) and CD95 (Percp-e710) were purchased from Thermo Fisher Scientific. Dead cells were excluded from flow cytometry analyses using a LIVE/DEAD Near-IR dye (Thermo Fisher Scientific). Horseradish peroxidase (HRP)–conjugated antibodies against mouse IgG, IgG1, IgG2a, IgG3, and IgM were purchased from Jackson ImmunoResearch. HRP-conjugated anti-mouse IgG2c was purchased from SouthernBiotech. Chloroquine used in in vivo experiments were purchased from Sigma and used at a dose of 10 mg/kg (intraperitoneally).

Infection of mice with parasitized RBCs

Parasites were grown from frozen infected RBC stocks in donor C57BL/6 mice. Peripheral blood parasitemia was checked using both blood smears and a flow cytometry–based strategy described elsewhere (*31*). Once parasitemia in donor mice reached a 5 to 10% range, blood drawn from the donor was diluted in phosphate-buffered saline (PBS) and injected to the experimental mice (intraperitoneally) at 10^{6} infected RBC per mouse unless otherwise noted. To avoid gradual changes in virulence by repetitive passaging of parasite, stocks prepared from comparable passage numbers were used. Progression of the blood-stage disease was monitored in the experimental mice by routine parasitemia checks as described above.

Construction of plasmid for editing AP2 (PBANKA_011210) in *Pb* NK65NYU

For editing the AP2 (PBANKA_011210) gene in *Pb* NK65NYU, replacing serine-1823 with phenylalanine (S1823F), we used the CRISPR-Cas9 system (*32*). A guide sequence of 20 nucleotides (5′-GCTGAATTAAAACCCCAAAG-3′), with protospacer adjacent motif (5′-AGG-3′), was selected by manual curation for targeting the Cas9 endonuclease to result in the desired editing (5467 TCT to TTT) in the AP2 gene. The 900 nucleotides of synthetic sequence (given in supplementary information 2) with the mutated guide region and the desired SNP (5467 TCT to TTT) were subcloned in the pYC plasmid using Nco I and Xho I restriction enzyme sites. The resulting plasmid, pYC_NK65AP2ANKA, was used for the transfection of the *Pb* NK65NYU parasites.

Transfection of the *Pb* NK65NYU parasites

The *Pb* transfections were done as described earlier (*33*, *34*). Briefly, a BALB/c mouse was infected with freshly revived frozen stock of *Pb* NK65NYU parasites. Two naïve BALB/c mice were injected intraperitoneally with the infected blood from the donor mouse (two to three drops of ~10% parasitemia). The mice were sacrificed once the parasitemia reached ~5%, and the parasites were allowed to develop in vitro to the mature schizont stage in RPMI 1640 with L-glutamine, 25 mM Hepes, and hypoxanthine (50 μg/ml; KD Medical, Columbia, MD), 28 ml of 7.5% sodium bicarbonate (KD Medical, Columbia, MD), and gentamicin (10 μg/ml; Gibco, Thermo Fisher Scientific, Grand Island, NY) supplemented with 20% fetal bovine serum. The mature schizont stage parasites were purified using Percoll purification method. The purified schizonts were washed twice with RPMI 1640 solution (KD Medicals, Columbia, MD). The schizonts (10^{6} to 10^{7}) were then resuspended in 100 μl of the Nucleofector solution prepared from Amaxa Basic Parasite Nucleofector Kit 1 (Lonza, USA) containing 10 μg of the

pYC_NK65AP2ANKA plasmid. The resuspended schizonts were transfected with Nucleofector II (Lonza, USA) using the program U33. The transfected parasites were mixed immediately with 100 µl of RPMI 1640 solution and injected intravenously in a naïve BALB/c mouse. The drug-resistant parasites were selected with pyrimethamine (0.7 mg/ml) and dissolved in the drinking water against the human dihydrofolate reductase selection marker in the transfected plasmid. The pyrimethamine treatment was continued for 1 week, and the drug-resistant parasites were screened for the presence of the desired SNP by DNA sequencing. The clonal parasite was generated by injecting 20 BALB/c mice with one parasite per mouse. The parasites were allowed to grow without pyrimethamine pressure. Once visible in the Giemsa smears, the parasites were passaged three times through C57BL/6 mice for the final study of the SNP in AP2. The WT NK65NYU parasites were also cycled in the BALB/c and C57BL/6 mice just like the edited parasites for comparative study.

Confirmation of editing in the AP2 gene (PBANKA_011210) of NK65NYU parasites by DNA sequencing

After the appearance of pyrimethamine-resistant parasites, the introduction of SNP in the AP2 gene of NK65NYU was confirmed by DNA sequencing. The genomic DNA from the AP2-mutated NK65NYU (*Pb*NK65^{F}) parasites was amplified with the following primer pair outside the 900-bp homology arm: AP2F (5′-GATTATAGATACAAATAATGAGAAAATGGG-3′) and AP2R (5′-GCATATGTGATAGTGTTATTTCCATC-3′). The introduction of the SNP was confirmed with two sequencing reactions performed using internal primers, one in forward (primer AP2Seq1, 5′-CAATTATAATAATTTGAATGAAGGGGAAC-3′) and another in reverse direction (primer AP2Seq2, 5′-GAGTAATCAAGAATCTCAAAATTGTGAT-3′).

To detect sequence inconsistencies between WT and CRISPR-modified samples, whole-genome sequencing was performed on TruSeq Nano (Illumina Inc.) paired-end libraries prepared from two WT (WT 81 and WT 83) and two mutant (AP2 76 and AP2 77) samples. Libraries were sequenced to a mean coverage of 172× on the NextSeq instrument using a 2× 150-cycle kit (Illumina Inc.).

Raw image files were converted to fastq files using bcl2fastq (v2.20.0.422, Illumina Inc., San Diego, CA), trimmed of adapter sequences, and quality-filtered for a minimum base quality score of 20 using cutadapt (v 1.12) (*35*) and FASTX (v 0.0.14) tools. Quality-trimmed reads were mapped to the *Pb NK65e* reference genome (assembly GCA_900088445.1) using Bowtie2 (version 2.2.9) (*36*). Bowtie2 default settings were used, with unpaired and discordant alignments suppressed. Reads were also mapped to mouse reference GRCm38/mm10 to assess contaminating mouse sequences. SAM files were converted to coordinate-sorted BAM files using SAMtools (*37*). Sequence read statistics are shown in table S1.

Duplicate reads were marked using Picard's MarkDuplicates tool (v 2.18.7) (*38*), and variants were detected in multisample mode using SAMtools and BCFtools packages with -ploidy 1 (*37*). In SAMtools, --redo-BAQ was enabled in mpileup. SNPs and INDELs were extracted into separate VCF files using GATK SelectVariants, and then each VCF file was filtered for depth and quality using vcftools (v 0.1.15) and –min-meanDP 10 and –minQ 200 parameters. The filtered multisample vcf file was annotated using SNPeff (*39*). Variants were also detected using GATK HaplotypeCaller and Freebayes, which yielded similar results.

Variants detected in the same position across all four samples, due to differences from the NK65e reference genome, were removed from further analysis. INDEL calls were concordant across all four samples, indicating that there were no differences in WT and mutant genomes. Raw sequences were submitted to the National Center for Biotechnology Information (NCBI) Sequence Read Archive database (accession no.: PRJNA548804).

Protein binding microarrays

Each *Pb* AP2 domain was PCR-amplified from *Pb* genomic DNA and cloned into the pGEX-4T1 vector (GE Healthcare) using Bam HI and Xho I restriction sites to create a gene fusion resulting in an N-terminal glutathione *S*-transferase (GST)–tagged recombinant protein. Protein expression was induced with 0.2 mM isopropyl-β-D-thiogalactopyranoside (IPTG) at 37°C for 4 hours in BL21-CodonPlus(DE3)-RIL cells (Agilent Technologies). Protein purification was carried out using Glutathione-Superflow Resin (Clontech), as previously described (*15*) and verified by Coomassie blue staining.

Purified recombinant proteins were run on protein binding microarrays (PBMs) to assess DNA binding activity, as previously described (*15*). Briefly, custom DNA microarrays (Agilent Technologies) were double-stranded, incubated with GST-tagged recombinant protein, incubated with Alexa 488–conjugated anti-GST antibody (Thermo Fisher Scientific, A11131), and scanned using an Axon 4300A scanner (Molecular Devices). Enrichment scores and position weight matrices (PWMs) were generated using seed-and-wobble algorithms from an earlier publication (*40*). Scores greater than 0.45 were considered significant and indicate specific binding.

Each GST-tagged protein was run on two PBM versions: AMADID 016060 (v9) and AMADID 015681 (v11). Each version contains the same oligonucleotide probes in a different order. PWMs from the two arrays were combined to generate the final results (data file S1).

Analysis of PWMs generated by in vitro PBMs was used to scan *Pb* promoter regions. First, PWMs were trimmed to their six most informative base pairs, or their core motifs. PlasmoDB version 34 (*41*) of the *Pb* ANKA reference genome and gene annotations were downloaded and used to generate promoters of 1500 nucleotides in length. Promoters were defined as 1500 bp upstream of the translation start site (ATG) of protein-coding genes only. These promoter regions were then scanned using FIMO version 4.12.0 (*42*) and a motif hit significance threshold of 0.001. Data analysis was performed in R version 3.4.1 (https://www.r-project.org). Analysis code is available at https://github.com/pzross/pberghei_ap2mutant.

Pb infection of mosquitoes

Anopheles stephensi female mosquitoes (5 to 6 days old) were infected with *Pb* by feeding on anesthetized infected C57BL/6 mice. The infectivity of the mice was established by determining the parasitemia in a blood smear. In all the studies, mice having parasitemias between 1 and 3% parasitemia were used to infect mosquitoes. Blood-fed infected mosquitoes were kept at 20°C and 80% humidity. *Pb* midgut infection was quantified by light microscopy 11 days after blood feeding with mercurochrome staining (0.1% in water). Sporozoite load was determined in salivary glands 21 days after blood feeding. The salivary glands of mosquitoes were dissected in PBS, and pools of 9 or 10 pairs of glands were homogenized by passaging through a

27-gauge needle 15 times. Sporozoites were counted under the microscope in a hemocytometer.

ELISA and serum cytokine analyses

To measure the relative amount of antibodies specific to parasite antigens, infected animals were bled at day 19 after infection. Blood was collected in anticoagulant tubes, spun down, washed with PBS, and then resuspended in approximately 4 ml of PBS. This solution was slowly added on top of a double Percoll gradient containing 40% Percoll (top) and 72% Percoll (bottom). Following ultracentrifugation, the middle layer containing enriched infected RBCs was harvested. Percoll was removed by washing the RBCs with RPMI mixed with 10× PBS at 10:1 and 20:1 ratios and RPMI alone for the first-second and third washes, respectively. iRBCs were pelleted and lysed in a buffer containing 100 mM tris (pH7.4), 150 mM NaCl, 1 mM phenylmethylsulfonyl fluoride, 1 mM EDTA, 1% Triton X-100, 0.5% sodium deoxycholate, and protease inhibitor cocktail (Roche) for 20 min on ice. Lysed cells were diluted with equal amount of PBS at the end of the procedure. For control group, RBCs from uninfected mice were harvested and lysed similarly. PBS solution containing 1:400 dilution of lysed RBC was used to coat Nunc Maxisorp enzyme-linked immunosorbent assay (ELISA) plates (Thermo Fisher Scientific). Upon overnight incubation at 4°C, plates were washed and blocked with bovine serum albumin–containing solution. Diluted sera harvested from infected animals were added to the wells followed by washing and incubation with HRP-conjugated secondary antibodies. Plates were developed using trimethylboron (TMB) solution, and reaction was terminated using 0.16 M H_2SO_4 solution. Plates were read at an optical density of 450 nm using a SpectraMax plate reader (Molecular Devices). Arbitrary units were calculated using a standard curve generated by applying serial dilutions of a mixed serum sample onto infected RBC lysate–coated wells.

Cytokine levels in sera of the infected animals were measured using relevant LEGENDplex kits (BioLegend) according to the manufacturer's guidelines.

Flow cytometry and histopathologic evaluation

For flow cytometry, samples were stained in Hanks' balanced salt solution supplemented with 2% fetal calf serum, 1% Hepes, and 10 mM sodium azide (Sigma-Aldrich). Analyses were carried out using a BD LSR-2 or a BD X20 cytometer. Data analysis was carried out using FlowJo software. Gating strategy for identifying different cell subsets was adapted from a previous study (*43*).

For histopathologic evaluation, spleens from infected mice were harvested at various time points after infection and immediately fixed in 10% formalin solution followed by embedding into paraffin. Tissue sections were either hematoxylin and eosin–stained or immunostained following a previously described protocol (*44*).

Quantitative reverse transcription PCR

Parasite loads in livers of sporozoite-injected (5×10^3 sporozoites per mouse, intravenously) mice were measured 45 hours after injection. Livers were flushed under anesthesia, and liver specimens were immediately frozen in liquid nitrogen. Livers were homogenized in RLT buffer using 2.3-mm zirconia/slica beads (Biospec) under agitation in a Biospec bead beater. Homogenate was further passed through QIAShredder (Qiagen) columns, and RNA was isolated using the RNeasy Plus Mini Kit (Qiagen) according to the manufacturer's guidelines. Complementary DNA (cDNA) synthesis was carried out using the iScript cDNA Synthesis Kit (Bio-Rad). qPCR was carried out using the IQ SYBR Green Kit (Bio-Rad). *Pb* 18*S* was amplified using two sets of primers: set 1 (5′-ATTAATCTTGAACGAGGAATGGCT-3′ and 5′-TCAATCGGTAGGAGCGACG-3′) and set 2 (5′-AAGCATTAAATAAAGCGAATACATCCTTAC-3′ and 5′-GGAGATTGGTTTTGACGTTTATGTG-3′). Three housekeeping genes murine HPRT (5′-TGCTCGAGATGTGATGAAGG-3′ and 5′-TCCCCTGTTGACTGGTCATT-3′), murine GAPDH (5′-GTGGAGTCATACTGGAACATGTAG-3′ and 5′-AATGGTGAAGGTCGGTGTG-3′), and murine PPIA (5′-TTCACCTTCCCAAAGACCAC-3′ and 5′-CAAACACAAACGGTTCCCAG-3′) were used for normalization. Delta C_t values were calculated by subtracting the geometric mean of C_t values of the three housekeeping genes from the C_t value of 18*S* for each sample.

RNA sequencing

For RNA sequencing, 250 µl of purified mouse cheek blood cells was mixed with 750 µl of Trizol LS (Thermo Fisher Scientific) and RNA was isolated according to the manufacturer's recommendations.

Twelve samples each containing 4 µg of total RNA were treated with the Globin-Zero Gold rRNA Removal Kit (Illumina Inc.) followed by TruSeq mRNA Sequencing Library Preparation (Illumina Inc.). The resulting single-indexed libraries were fragment-sized on a Bioanalyzer DNA1000 chip and quantitated using a Kapa Library Quant kit (Illumina) and Universal qPCR mix (Roche) to facilitate the creation of a normalized, 2 nM multiplexed pool. This multiplexed pool was clustered across two lanes of a RAPID flow cell at a concentration of 10 pM, followed by paired-end sequencing on an Illumina HiSeq 2500 for 100 cycles from each fragment end plus an additional 7 cycles to sequence the index.

Raw next generation sequencing (NGS) reads were processed by first removing any Illumina adapter sequences using Cutadapt v1.12 (*35*) and then trimmed and filtered for quality and length (minimum length of 35 bp) using FastX Tool Kit v0.0.14 (Hannon Lab, Cold Spring Harbor Laboratory). Trimmed reads for each replicate were then mapped using Hisat2 v2.0.5 (*45*) set to report only matched pairs. Final transcripts based on the combined replicates and then differentials for each comparison were generated using Deseq2 (10.18129/B9.bioc.DESeq2) for each experimental condition. RNA-seq data were uploaded to the NCBI Gene Expression Omnibus repository with the accession number GSE111333.

SUPPLEMENTARY MATERIALS

Supplementary material for this article is available at http://advances.sciencemag.org/cgi/content/full/6/6/eaaw6957/DC1

Fig. S1. CRISPR-Cas9 gene modification strategy is outlined.

Fig. S2. The SNP in PBANKA_011210 ApiAP2 TF does not interfere with the progression of sexual and pre-erythrocytic stages of the *P. berghei* life cycle.

Fig. S3. Flow cytometry gating strategy.

Fig. S4. Graphs comparing mice infected with *Pb*NK65^F and *Pb*NK65^S.

Table S1. Summary of changes observed between the WT and CRISPR-Cas9–mutated parasites based on whole-genome sequencing analysis.

Supplementary information 2. The 900-nucleotide synthetic sequence.

Data file S1. Supplementary information 1: DNA binding analysis of ApiAP2 domain 1.

REFERENCES AND NOTES

1. World Health Organization, *WHO World Malaria Report* (World Health Organization, 2017).
2. W. E. Collins, G. M. Jeffery, A retrospective examination of secondary sporozoite- and trophozoite-induced infections with Plasmodium falciparum: Development of

parasitologic and clinical immunity following secondary infection. *Am. J. Trop. Med. Hyg.* **61**, 20–35 (1999).
3. N. P. Day, T. T. Hien, T. Schollaardt, P. P. Loc, L. V. Chuong, T. T. Chau, N. T. Mai, N. H. Phu, D. X. Sinh, N. J. White, M. Ho, The prognostic and pathophysiologic role of pro- and antiinflammatory cytokines in severe malaria. *J. Infect. Dis.* **180**, 1288–1297 (1999).
4. K. E. Lyke, R. Burges, Y. Cissoko, L. Sangare, M. Dao, I. Diarra, A. Kone, R. Harley, C. V. Plowe, O. K. Doumbo, M. B. Sztein, Serum levels of the proinflammatory cytokines interleukin-1 beta (IL-1beta), IL-6, IL-8, IL-10, tumor necrosis factor alpha, and IL-12(p70) in Malian children with severe Plasmodium falciparum malaria and matched uncomplicated malaria or healthy controls. *Infect. Immun.* **72**, 5630–5637 (2004).
5. M. Walther, J. Woodruff, F. Edele, D. Jeffries, J. E. Tongren, E. King, L. Andrews, P. Bejon, S. C. Gilbert, J. B. de Souza, R. Sinden, A. V. S. Hill, E. M. Riley, Innate immune responses to human malaria: Heterogeneous cytokine responses to blood-stage Plasmodium falciparum correlate with parasitological and clinical outcomes. *J. Immunol.* **177**, 5736–5745 (2006).
6. B. C. Urban, R. Ing, M. M. Stevenson, Early interactions between blood-stage plasmodium parasites and the immune system. *Curr. Top. Microbiol. Immunol.* **297**, 25–70 (2005).
7. J. Langhorne, F. M. Ndungu, A. M. Sponaas, K. Marsh, Immunity to malaria: More questions than answers. *Nat. Immunol.* **9**, 725–732 (2008).
8. J. M. Batchelder, J. M. Burns Jr., F. K. Cigel, H. Lieberg, D. D. Manning, B. J. Pepper, D. M. Yañez, H. van der Heyde, W. P. Weidanz, Plasmodium chabaudi adami: Interferon-gamma but not IL-2 is essential for the expression of cell-mediated immunity against blood-stage parasites in mice. *Exp. Parasitol.* **105**, 159–166 (2003).
9. J. L. Grun, W. P. Weidanz, Immunity to Plasmodium chabaudi adami in the B-cell-deficient mouse. *Nature* **290**, 143–145 (1981).
10. J. Langhorne, C. Cross, E. Seixas, C. Li, T. von der Weid, A role for B cells in the development of T cell helper function in a malaria infection in mice. *Proc. Natl. Acad. Sci. U.S.A.* **95**, 1730–1734 (1998).
11. A. Scholzen, R. W. Sauerwein, How malaria modulates memory: Activation and dysregulation of B cells in Plasmodium infection. *Trends Parasitol.* **29**, 252–262 (2013).
12. D. Perez-Mazliah, J. Langhorne, CD4 T-cell subsets in malaria: TH1/TH2 revisited. *Front. Immunol.* **5**, 671 (2014).
13. K. Witmer, C. D. Schmid, N. M. B. Brancucci, Y. H. Luah, P. R. Preiser, Z. Bozdech, T. S. Voss, Analysis of subtelomeric virulence gene families in Plasmodium falciparum by comparative transcriptional profiling. *Mol. Microbiol.* **84**, 243–259 (2012).
14. T. D. Otto, U. Böhme, A. P. Jackson, M. Hunt, B. Franke-Fayard, W. A. M. Hoeijmakers, A. A. Religa, L. Robertson, M. Sanders, S. A. Ogun, D. Cunningham, A. Erhart, O. Billker, S. M. Khan, H. G. Stunnenberg, J. Langhorne, A. A. Holder, A. P. Waters, C. I. Newbold, A. Pain, M. Berriman, C. J. Janse, A comprehensive evaluation of rodent malaria parasite genomes and gene expression. *BMC Biol.* **12**, 86 (2014).
15. T. L. Campbell, E. K. De Silva, K. L. Olszewski, O. Elemento, M. Llinás, Identification and genome-wide prediction of DNA binding specificities for the ApiAP2 family of regulators from the malaria parasite. *PLOS Pathog.* **6**, e1001165 (2010).
16. S. Balaji, M. M. Babu, L. M. Iyer, L. Aravind, Discovery of the principal specific transcription factors of Apicomplexa and their implication for the evolution of the AP2-integrase DNA binding domains. *Nucleic Acids Res.* **33**, 3994–4006 (2005).
17. H. J. Painter, T. L. Campbell, M. Llinás, The Apicomplexan AP2 family: Integral factors regulating Plasmodium development. *Mol. Biochem. Parasitol.* **176**, 1–7 (2011).
18. K. Modrzynska, C. Pfander, L. Chappell, L. Yu, C. Suarez, K. Dundas, A. R. Gomes, D. Goulding, J. C. Rayner, J. Choudhary, O. Billker, A knockout screen of ApiAP2 genes reveals networks of interacting transcriptional regulators controlling the plasmodium life cycle. *Cell Host Microbe* **21**, 11–22 (2017).
19. A. Sinha, Thesis, University of Glasgow, Glasgow, UK (2014).
20. D. Cunningham, J. Lawton, W. Jarra, P. Preiser, J. Langhorne, The pir multigene family of Plasmodium: Antigenic variation and beyond. *Mol. Biochem. Parasitol.* **170**, 65–73 (2010).
21. M. Zeeshan, R. K. Tyagi, K. Tyagi, M. S. Alam, Y. D. Sharma, Host-parasite interaction: Selective Pv-fam-a family proteins of Plasmodium vivax bind to a restricted number of human erythrocyte receptors. *J. Infect. Dis.* **211**, 1111–1120 (2015).
22. M. Zeeshan, K. Tyagi, Y. D. Sharma, CD4+ T cell response correlates with naturally acquired antibodies against Plasmodium vivax tryptophan-rich antigens. *Infect. Immun.* **83**, 2018–2029 (2015).
23. J. J. Guthmiller, A. C. Graham, R. A. Zander, R. L. Pope, N. S. Butler, Cutting Edge: IL-10 is essential for the generation of germinal center b cell responses and anti-plasmodium humoral immunity. *J. Immunol.* **198**, 617–622 (2017).
24. E. T. Cadman, A. Y. Abdallah, C. Voisine, A. M. Sponaas, P. Corran, T. Lamb, D. Brown, F. Ndungu, J. Langhorne, Alterations of splenic architecture in malaria are induced independently of Toll-like receptors 2, 4, and 9 or MyD88 and may affect antibody affinity. *Infect. Immun.* **76**, 3924–3931 (2008).
25. J. Krucken, L. I. Mehnert, M. A. Dkhil, M. El-Khadragy, W. P. M. Benten, H. Mossmann, F. Wunderlich, Massive destruction of malaria-parasitized red blood cells despite spleen closure. *Infect. Immun.* **73**, 6390–6398 (2005).
26. M. M. Stevenson, G. Kraal, Histological changes in the spleen and liver of C57BL/6 and A/J mice during Plasmodium chabaudi AS infection. *Exp. Mol. Pathol.* **51**, 80–95 (1989).
27. C. Fernandez-Arias, J. Rivera-Correa, J. Gallego-Delgado, R. Rudlaff, C. Fernandez, C. Roussel, A. Götz, S. Gonzalez, A. Mohanty, S. Mohanty, S. Wassmer, P. Buffet, P. A. Ndour, A. Rodriguez, Anti-self phosphatidylserine antibodies recognize uninfected erythrocytes promoting malarial anemia. *Cell Host Microbe* **19**, 194–203 (2016).
28. J. Rivera-Correa, J. J. Guthmiller, R. Vijay, C. Fernandez-Arias, M. A. Pardo-Ruge, S. Gonzalez, N. S. Butler, A. Rodriguez, Plasmodium DNA-mediated TLR9 activation of T-bet^{+} B cells contributes to autoimmune anaemia during malaria. *Nat. Commun.* **8**, 1282 (2017).
29. World Health Organization, *World Malaria Report 2016* (World Health Organization, 2016).
30. P. J. Spence, W. Jarra, P. Lévy, A. J. Reid, L. Chappell, T. Brugat, M. Sanders, M. Berriman, J. Langhorne, Vector transmission regulates immune control of Plasmodium virulence. *Nature* **498**, 228–231 (2013).
31. E. B. Gordon, G. T. Hart, T. M. Tran, M. Waisberg, M. Akkaya, J. Skinner, S. Zinöcker, M. Pena, T. Yazew, C. F. Qi, L. H. Miller, S. K. Pierce, Inhibiting the mammalian target of rapamycin blocks the development of experimental cerebral malaria. *MBio* **6**, e00725 (2015).
32. C. Zhang, B. Xiao, Y. Jiang, Y. Zhao, Z. Li, H. Gao, Y. Ling, J. Wei, S. Li, M. Lu, X. Z. Su, H. Cui, J. Yuan, Efficient editing of malaria parasite genome using the CRISPR/Cas9 system. *MBio* **5**, e01414 (2014).
33. C. J. Janse, J. Ramesar, A. P. Waters, High-efficiency transfection and drug selection of genetically transformed blood stages of the rodent malaria parasite Plasmodium berghei. *Nat. Protoc.* **1**, 346–356 (2006).
34. A. P. Waters, A. W. Thomas, M. R. van Dijk, C. J. Janse, Transfection of malaria parasites. *Methods* **13**, 134–147 (1997).
35. M. Martin, Cutadapt removes adapter sequences from high-throughput sequencing reads. *EMBnet J.* **17**, 10–12 (2011).
36. B. Langmead, S. L. Salzberg, Fast gapped-read alignment with Bowtie 2. *Nat. Methods* **9**, 357–359 (2012).
37. H. Li, A statistical framework for SNP calling, mutation discovery, association mapping and population genetical parameter estimation from sequencing data. *Bioinformatics* **27**, 2987–2993 (2011).
38. Broad Institute, http://broadinstitute.github.io/picard/ (2018).
39. P. Cingolani, A. Platts, L. L. Wang, M. Coon, T. Nguyen, L. Wang, S. J. Land, X. Lu, D. M. Ruden, A program for annotating and predicting the effects of single nucleotide polymorphisms, SnpEff: SNPs in the genome of Drosophila melanogaster strain w1118; iso-2; iso-3. *Fly* **6**, 80–92 (2012).
40. M. F. Berger, M. L. Bulyk, Universal protein-binding microarrays for the comprehensive characterization of the DNA-binding specificities of transcription factors. *Nat. Protoc.* **4**, 393–411 (2009).
41. C. Aurrecoechea, J. Brestelli, B. P. Brunk, J. Dommer, S. Fischer, B. Gajria, X. Gao, A. Gingle, G. Grant, O. S. Harb, M. Heiges, F. Innamorato, J. Iodice, J. C. Kissinger, E. Kraemer, W. Li, J. A. Miller, V. Nayak, C. Pennington, D. F. Pinney, D. S. Roos, C. Ross, C. J. Stoeckert, C. Treatman, H. Wang, PlasmoDB: A functional genomic database for malaria parasites. *Nucleic Acids Res.* **37**, D539–D543 (2009).
42. C. E. Grant, T. L. Bailey, W. S. Noble, FIMO: Scanning for occurrences of a given motif. *Bioinformatics* **27**, 1017–1018 (2011).
43. M. Akkaya, B. Akkaya, A. S. Kim, P. Miozzo, H. Sohn, M. Pena, A. S. Roesler, B. P. Theall, T. Henke, J. Kabat, J. Lu, D. W. Dorward, E. Dahlstrom, J. Skinner, L. H. Miller, S. K. Pierce, Toll-like receptor 9 antagonizes antibody affinity maturation. *Nat. Immunol.* **19**, 255–266 (2018).
44. M. Akkaya, B. Akkaya, P. W. Sheehan, P. Miozzo, M. Pena, C. F. Qi, J. Manzella-Lapeira, S. Bolland, S. K. Pierce, T cell-dependent antigen adjuvanted with DOTAP-CpG-B but not DOTAP-CpG-A induces robust germinal center responses and high affinity antibodies in mice. *Eur. J. Immunol.* **47**, 1890–1899 (2017).
45. D. Kim, B. Langmead, S. L. Salzberg, HISAT: A fast spliced aligner with low memory requirements. *Nat. Methods* **12**, 357–360 (2015).

Acknowledgments
Funding: This work was supported by the Intramural Research Program of the NIH, National Institute of Allergy and Infectious Diseases. L.M.O. and M.L. were funded by NIH grant R01AI125565. **Author contributions:** Conceived the project: S.K.P., M.A.,

L.H.M., A.B., and O.B.; secured funding: S.K.P. and L.H.M.; designed the experiments: M.A., A.B., P.W.S., A.M.-C., S.K.P., and L.H.M.; carried out the experiments: M.A., A.B., P.W.S., C.K.C., L.M.O., T.D.O., G.T., M.P., T.Y., and A.M.-C.; analyzed data: M.A., P.W.S., A.B., M.L., P.R., D.S., C.-F.Q., A.M.-C., and S.L.A.; wrote the manuscript: M.A. and S.K.P.; edited the manuscript: L.H.M., M.L., and O.B. **Competing interest:** The authors declare that they have no competing interests. **Data and materials availability:** All data needed to evaluate the conclusions in the paper are present in the paper and/or the Supplementary Materials. Additional data related to this paper may be requested from the authors.

Submitted 16 January 2019
Accepted 21 November 2019
Published 5 February 2020
10.1126/sciadv.aaw6957

Citation: M. Akkaya, A. Bansal, P. W. Sheehan, M. Pena, A. Molina-Cruz, L. M. Orchard, C. K. Cimperman, C.-F. Qi, P. Ross, T. Yazew, D. Sturdevant, S. L. Anzick, G. Thiruvengadam, T. D. Otto, O. Billker, M. Llinás, L. H. Miller, S. K. Pierce, A single-nucleotide polymorphism in a *Plasmodium berghei* ApiAP2 transcription factor alters the development of host immunity. *Sci. Adv.* **6**, eaaw6957 (2020).